those of polycrystalline switchable mirrors evaporated on sapphire[8] (A. T. M. van Gogh, manuscript in preparation). Such films are not epitaxial but only show a texture with the *c*-axis out of plane. Although *in situ* X-ray studies revealed the existence of two coexisting phase regions ($Y–YH_2$ and $YH_2–YH_3$), no optical inhomogeneity was observed[8]. This is most likely to be due to the small size of their domain structure[17,18].

The self-organized, switchable tile pattern of epitaxial switchable mirrors suggests potential applications. A switchable mirror can be integrated in an all-solid-state device[6] (P. van der Sluis *et al.*, manuscript in preparation), so the switching tiles could be treated as individually addressable pixels in an optical display. Furthermore, the reversible, dramatic out-of-plane height variation (9.3%) offers potential for high-load (in the order of GPa) micromechanical actuators of far smaller dimensions than devices based on piezoelectric expansion.

One of the prerequisites for such devices is a dense and regular pixel pattern with a tunable domain size. One way to tune the domain size follows from Fig. 4 which shows that ridge spacing d and ridge height h increase linearly with film thickness t. The observed trend and magnitude can be understood in terms of a partially clamped film, in which the stress relaxation caused by one ridge has a limited functional range. The ridge network is created by the 0.8% in-plane expansion during the $Y–YH_2$ transition: the constraint by the substrate leads to large compressive stresses which are released by pushing some material outward in the form of ridges[7]. The measured volume of the ridges accounts for all the excess material. At the same time, the relatively wide spacing (in the order of μm) of the ridges implies significant in-plane material transport. This occurs through gliding of the plastic metallic film over the rigid substrate and release of the excess material at the ridges by plastic deformation. The onset of film sliding is determined by a critical shear γ_i between the film and the substrate. Analogously, the onset of ridge creation is determined by a critical stress σ_r. As soon as a given ridge is formed, it instantaneously lowers in its vicinity the average compressive stress $\sigma(x)$, just as a crack reduces local tensile stress[19]. Assuming a constant critical interface shear γ_i, the stress $\sigma(x)$ increases linearly away from the ridge, until it reaches the critical value σ_r at a certain distance. If the stress relief at the ridge is maximum, it follows that one ridge has a limited functional range around it, given by $d = 2t(\sigma_r/\gamma_i)$: the separation between the ridges d depends on the film thickness t scaled by the ratio $2\sigma_r/\gamma_i$. For any chosen crystal plane at an angle α with the film plane, σ_r corresponds to a critical shear $\gamma_p = \sigma_r \cos(\alpha)\sin(\alpha)$ along this plane. This yields $d = Ct$ with $C = 4(\gamma_p/\gamma_i)/\sin(2\alpha)$. Assuming $\gamma_p \approx \gamma_i$, we find that $C \gtrsim 4$ for any plane. For hexagonal yttrium, a plausible choice is the $(1\bar{1}02)$ twinning plane, at an angle α of 42.2° with the film surface (using measured lattice spacings[7]). This particular plane yields $C = 4$, consistent with the measured value of 3.7 ± 0.6 (see Fig. 4b). Moreover, a double twin (see Fig. 4a) creates asymmetric ridges with a steepest slope of $2(45 - \alpha) = 5.6$ degrees, in nice agreement with the measured (see also Fig. 3) average steepest slope of (5.8 ± 0.2) degrees.

Thus a fundamentally and technologically very attractive behaviour occurs in epitaxial switchable mirrors: single-domain phase switching. The effect takes place because the first loading of an epitaxial YH_x/CaF_2 film generates a self-organized, closed ridge structure which blocks hydrogen diffusion and accommodates completely plastic deformation. The domains defined by the ridge network switch homogeneously and independently. The possibility of generating a tunable, dense pattern of switchable pixels opens the way to solid state displays based on switchable mirrors. □

Received 7 February; accepted 8 June 2000.

1. Huiberts, J. N. *et al.* Yttrium and lanthanum hydride films with switchable optical properties. *Nature* **380,** 231–234 (1996).
2. Kelly, P. J., Dekker, J. P. & Stumpf, R. Theoretical prediction of the structure of insulating YH_3. *Phys. Rev. Lett.* **78,** 1315–1318 (1997).
3. Ng, K. K., Zhang, F. C., Anisimov, V. I. & Rice, T. M. Theory for metal hydrides with switchable optical properties. *Phys. Rev. B* **59,** 5398–5413 (1999).
4. Eder, R., Pen, H. A. & Sawatzky, G. A. Kondo-lattice-like effects of hydrogen in transition metals. *Phys. Rev. B* **56,** 10115–10120 (1997).
5. den Broeder, F. J. A. *et al.* Visualization of hydrogen migration in solids using switchable mirrors. *Nature* **394,** 656–658 (1998).
6. Armitage, R., Rubin, M., Richardson, T., O'Brien, N. & Chen, Y. Solid-state gadolinium–magnesium hydride optical switch. *Appl. Phys. Lett.* **75,** 1863–1865 (1999).
7. Nagengast, D. G., Kerssemakers, J. W. J., van Gogh, A. T. M., Dam, B. & Griessen, R. Epitaxial switchable yttrium-hydride mirrors. *Appl. Phys. Lett.* **75,** 1724–1726 (1999).
8. Kremers, M. *et al.* Optical transmission spectroscopy of switchable yttrium hydride films. *Phys. Rev. B* **57,** 4943–4949 (1998).
9. van der Sluis, P., Ouwerkerk, M. & Duine, P. A. Optical switches based on magnesium lanthanide alloy hydrides. *Appl. Phys. Lett.* **70,** 3356–3358 (1997).
10. van Gogh, A. T. M., Kooij, E. S. & Griessen, R. Isotope effects in switchable metal-hydride mirrors. *Phys. Rev. Lett.* **83,** 4614–4617 (1999).
11. Hayoz, J. *et al.* Observation of the reversible H-induced structural transition in thin Y films via x-ray photoelectron diffraction. *Phys. Rev. B* **58,** R4270–R4273 (1998).
12. Remhof, A. *et al.* Hydrogen and deuterium in epitaxial Y(0001) films: Structural properties and isotope exchange. *Phys. Rev. B* **59,** 6689–6699 (1999).
13. Grier, E. J. *et al.* Structural changes to epitaxial (0001) holmium layers during hydrogen loading. *J. Phys. D* **33,** 894–900 (2000).
14. Kooij, E. S., van Gogh, A. T. M. & Griessen, R. In situ resistivity measurements and optical transmission and reflection spectroscopy of electrochemically loaded switchable YH_x films. *J. Electrochem. Soc.* **146,** 2990–2994 (1999).
15. Vajda, P. in *Handbook on the Physics and Chemistry of Rare Earths* Ch. 20 (eds Gschneider, K. A. & Eyring, L.) 207–291 (Elsevier, Amsterdam, 1995).
16. Remhof, A. *et al.* In-situ x-ray diffraction topography studies on the phase formation in thin yttrium hydride films. *Phys. Rev. B* (in the press).
17. van der Molen, S. J. *et al.* Hydriding kinetics of Pd capped YHx switchable mirrors. *J. Appl. Phys.* **86,** 6107–6119 (1999).
18. Huiberts, J. N. *et al.* Synthesis of yttrium trihydride films for ex-situ measurements. *J. Alloys Compounds* **239,** 158–171 (1996).
19. Hu, M. S. & Evans, A. G. The cracking and decohesion of thin films on ductile substrates. *Acta Metall.* **37,** 17–925 (1989).

Acknowledgements

We thank B. Dam, D. Nagengast, M. van Gogh, M. Welling, R. Elberse, A. Pundt and P. van der Sluis for support, advice and discussions. This work was supported by the Stichting voor Fundamenteel Onderzoek der Materie (FOM), which is financed by NWO. We also acknowledge financial contribution from the European Commission through the TMR program (research network 'Switchable metal hydride films').

Correspondence and requests for materials should be addressed to R.G. (e-mail: kers@nat.vu.nl).

Electrostatic trapping of ammonia molecules

Hendrick L. Bethlem, Giel Berden, Floris M. H. Crompvoets, Rienk T. Jongma, André J. A. van Roij & Gerard Meijer

FOM-Institute for Plasma Physics Rijnhuizen, PO Box 1207, NL-3430 BE Nieuwegein, The Netherlands, and Department of Molecular and Laser Physics, University of Nijmegen, Toernooiveld 1, NL-6525 ED Nijmegen, The Netherlands

The ability to cool and slow atoms with light for subsequent trapping[1–3] allows investigations of the properties and interactions of the trapped atoms in unprecedented detail. By contrast, the complex structure of molecules prohibits this type of manipulation, but magnetic trapping of calcium hydride molecules thermalized in ultra-cold buffer gas[4] and optical trapping of caesium dimers[5] generated from ultra-cold caesium atoms have been reported. However, these methods depend on the target molecules being paramagnetic or able to form through the association of atoms amenable to laser cooling[6–8], respectively, thus restricting the range of species that can be studied. Here we describe the slowing of an adiabatically cooled beam of deuterated ammonia molecules by time-varying inhomogeneous electric fields[9,10] and subsequent loading into an electrostatic trap. We

are able to trap state-selected ammonia molecules with a density of 10^6 cm^{-3} in a volume of 0.25 cm^3 at temperatures below 0.35 K. We observe pronounced density oscillations caused by the rapid switching of the electric fields during loading of the trap. Our findings illustrate that polar molecules can be efficiently cooled and trapped, thus providing an opportunity to study collisions and collective quantum effects in a wide range of ultra-cold molecular systems[11–14].

Adiabatic cooling in an expansion can be used to obtain high densities of cold molecules. In pulsed molecular beams, densities on the order of 10^{12} molecules per cm^3 in a single quantum state at translational temperatures of 1 K are readily achieved. Typical velocities in a molecular beam are in the 250–2,000 m s^{-1} range, however, preventing trapping of these dense low-temperature samples in the laboratory frame. Various methods are currently being explored to translate the high phase-space densities from the moving frame of the molecular beam to the laboratory frame[9,10,15–17]. Once molecules are present at sufficiently low kinetic energies they can be trapped in various ways, for instance, by using the rather deep traps (~1 K) that can be formed with inhomogeneous magnetic[18] or electric fields[19].

Our approach to slowing down and trapping a beam of neutral molecules exploits the interaction of dipolar molecules with electric fields. The experimental set-up consists of a compact molecular beam machine, schematically indicated in Fig. 1. A pulsed beam of ND_3 is produced by expanding a mixture of less than 1% ND_3 (where D is deuterium) in Xe into vacuum, using a modified solenoid valve. Seeding of ND_3 in the heaviest rare gas, together with cooling of the pulsed valve, results in a mean beam velocity of 280 m s^{-1} (kinetic energy E_{kin} = 66 cm^{-1}). The velocity spread is approximately 15%, corresponding to a translational temperature of about 0.8 K in the moving frame. Only molecules in states that gain Stark energy with increasing electric field, that is, molecules in so-called 'low-field seeking' states, are selected in these experiments. The only low-field seeking state populated in the molecular beam is the $|J\,K\,|M|\rangle = |1\,1\,1\rangle$ upper inversion level in the vibrational ground state: approximately one-eighth of the total number of ND_3 molecules is in this particular quantum state. The electric dipole moment of ND_3 is 1.5 debye (ref. 20), and molecules in this particular level experience a positive Stark shift of 1.2 cm^{-1} in an electric field of 100 kV cm^{-1}. We selected ND_3 rather than NH_3 for these experiments because the magnitude of the inversion splitting is significantly reduced upon deuteration, resulting in a more linear Stark effect for ND_3 in the applied electric fields[20].

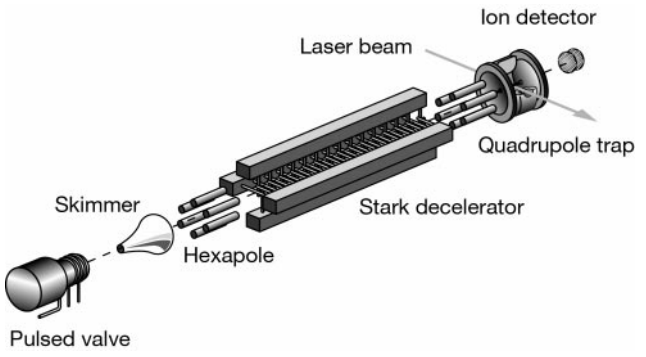

Figure 1 Experimental set-up. From left to right a gas pulse of ND_3 in Xe exits a cooled (T = 200 K) pulsed valve with a mean velocity of 280 m s^{-1}. After passage through the skimmer the beam is collimated with a pulsed hexapole and a subset of these molecules is subsequently slowed down upon passage through the Stark decelerator. The package of slow molecules is focused into the electrostatic trap. Part of the ring electrode is not drawn to allow a view of the inside of the trap. Molecules at the centre of the trap are ionized with the laser; ions are extracted and detected with an ion detector. The flight path of the molecules from the pulsed valve to the centre of the trap is 56 cm.

The ND_3 molecules pass through a 1.0-mm diameter skimmer into a second, differentially pumped, vacuum chamber and fly into a short pulsed hexapole that acts as a positive lens for the selected ND_3 molecules. After exiting the hexapole the molecules enter a 35-cm long Stark decelerator. The decelerator consists of an array of 63 equidistant electric field stages. When the state-selected ND_3 molecules enter a region of high electric field (typically up to 100 kV cm^{-1}), they will gain Stark energy. This gain in Stark energy ('potential' energy) is compensated by a loss in kinetic energy. If the electric field is greatly reduced before the molecules have left this region they will not regain the lost kinetic energy. This process is repeated by letting the molecules pass through the series of electric field stages, which are switched synchronously with the arrival of the package of decelerating molecules in these stages. This provides a method of decelerating a sample of neutral molecules while maintaining the initial phase-space density[9,10], much as is done in charged-particle accelerators.

A second pulsed hexapole at the end of the decelerator focuses the slow molecules exiting the decelerator into the electrostatic trap. The trap has a quadrupole geometry[19] and a cut through the centre of the trap is shown in the upper part of Fig. 2. The 2-mm diameter entrance and exit holes in the end-caps enable the molecular beam to pass through the trap. The inner radius of the ring electrode is 5 mm. There are 2-mm diameter holes in this electrode to allow probing of the density of ND_3 molecules at the centre of the trap via a laser-ionization detection scheme. Using the focused radiation of a pulsed laser at 302.4 nm, only the ND_3 molecules in the selected state are multi-photon ionized[21]. Just before the probe laser is fired, the voltages on the entrance end-cap as well as on the ring electrode are switched off. A constant voltage of −400 V is applied to the exit end-cap. The trap thus serves as the extraction region of a linear time-of-flight mass spectrometer, and the ND_3-ion signal is recorded using an ion detector placed further downstream.

In order to transport the molecules into the quadrupole trap, some residual velocity is required. In the lower trace of Fig. 3, the arrival-time distribution of decelerated ND_3 molecules at the centre of the trap is shown relative to the time when the pulsed valve is opened. No voltages are applied to the entrance end-cap and ring

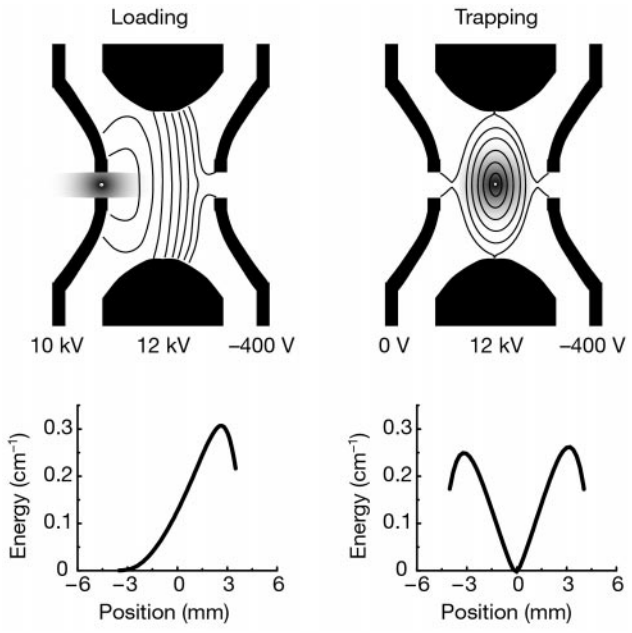

Figure 2 Configuration of the trap with the voltages as applied during loading and trapping. In the trap, lines of equal electric field are indicated and the cloud of molecules is sketched. The potential energy along the molecular beam axis of the ND_3 molecules in the $|J\,K\rangle = |1\,1\rangle$ state with positive Stark shift is shown for both field geometries.

electrode. In this particular case, the Stark decelerator is set to decrease the kinetic energy of the ND_3 molecules by about 0.9 cm^{-1} per electric field stage, starting from an initial mean velocity of 260 m s^{-1} (E_{kin} = 57 cm^{-1}). It should be noted that only 1% of the ND_3 molecules in the molecular beam that are in the right quantum-state are also in the region of phase-space that is accepted by the Stark decelerator with these settings. The mean velocity of the package of slow molecules arriving at the centre of the trap at 7.7 ms is 13 m s^{-1} (E_{kin} = 0.13 cm^{-1}), and has a relatively narrow velocity spread of 2 m s^{-1} at full-width half-maximum (FWHM). The latter corresponds to a translational temperature in the moving frame of the order of 2 mK.

To load the trap, the voltages on the trap are applied asymmetrically, as shown in Fig. 2. The ND_3 molecules thus have to climb a last potential hill, and are brought to a standstill near the centre of the trap. The measured density of the ND_3 molecules at the centre of the trap as a function of time in this field geometry is shown in the middle trace of Fig. 3. As expected, the molecules are observed to reach the centre of the trap somewhat later. Basically, the data show the reflection of the slow molecules from the repulsive wall ('concave mirror') of the trap.

To actually trap the molecules, we switch the voltage on the entrance end-cap to ground potential when the molecules have come to a near-standstill inside the trap. We thereby create a (near) symmetric electric field configuration with a minimum at the geometrical centre of the trap. The depth of the potential well in which the ND_3 molecules are then confined is 0.24 cm^{-1} (0.35 K), giving a strict upper limit to the temperature of the sample of trapped molecules. Depending on the details of the trap-loading, the actual temperature of the molecules in the trap might be as low as the translational temperature originally present in the moving frame of the decelerated molecular beam. The measured density of ND_3 at the centre of the trap as a function of time is shown in the upper trace of Fig. 3. At early times after switching on the trap, clear oscillations in the density with a period of 0.58 ms are observed. These oscillations are a signature of the bouncing of the molecules in the three-dimensional potential well when still only a relatively small region of space is occupied by the trapped molecules. The oscillations fade away after several milliseconds and a steady signal from the trapped ND_3 molecules remains. The actual signal observed from the trapped molecules amounts to a few ND_3 ions per laser pulse. As ionization of the trapped ND_3 molecules only takes place in the focus of the laser beam, and as the resulting ions have to be extracted through the 2-mm diameter hole in the exit end-cap, the actual detection volume is less than 10^{-5} cm^3. This translates into a lower limit for the density of trapped, state-selected ammonia molecules of 10^6 cm^{-3}.

To determine the trapping lifetime, the ND_3 density at the centre of the trap is monitored as a function of the time elapsed since loading of the trap. The results are displayed in the inset of Fig. 3. An exponential decay of the number of trapped molecules with a $1/e$ decay time of 0.24 ± 0.04 s is observed. The measured background pressure in the vacuum chamber is around 2×10^{-8} mbar, and collisions with background-gas are therefore most probably responsible for the observed trap-loss rate. Owing to the increased pressure in the chamber shortly after releasing the gas pulse, the trap loss rate is observed to be slightly higher at early trapping times.

The deceleration and trapping scheme presented here can be applied to a large variety of neutral molecules. For this, the molecule under study must have a sufficiently large positive Stark shift (about 1 cm^{-1}) in experimentally feasible electric fields (about 200 kV cm^{-1}). Furthermore, a pulsed beam with sufficiently low initial kinetic energy is required. On the basis of these criteria, molecules such as OH, NH($a^1\Delta$), NO, CO($a^3\Pi$), H_2O, NO_2, H_2CO and CH_3F appear to be excellent candidates for future trapping experiments. It is expected that the trapped molecules can then be further cooled using evaporative cooling or using laser-cooling on ro-vibrational transitions. This opens the way for the study of cold molecule–molecule collisions, collective quantum effects in molecular systems, the physics of mutually interacting dipolar molecules and many other applications already realized for atoms[18,22]. □

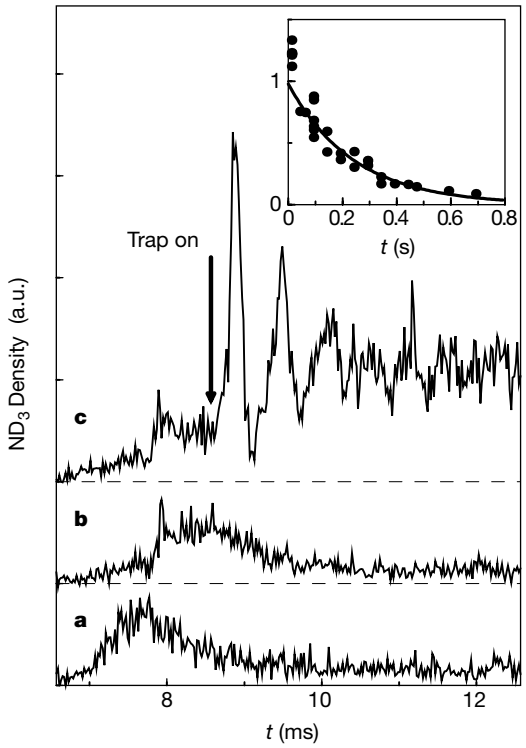

Figure 3 Density of ammonia molecules at the centre of the trap as a function of time. The horizontal axis shows the time after opening of the pulsed valve. **a**–**c**, The three traces show the ND_3 density at the centre of the trap when no voltages are applied to the entrance end-cap and the ring electrode (**a**), when voltages are applied as depicted for the loading scheme in Fig. 2 (**b**) and when voltages are applied for loading and trapping (**c**). The time that switching from the loading to the trapping scheme occurs is indicated by an arrow. The inset shows the density of trapped ammonia molecules on a longer timescale. The dashed curve shows an exponential curve with a $1/e$ decay time of 0.24 s.

Received 30 May; accepted 30 June 2000.

1. Chu, S. Manipulation of neutral particles. *Rev. Mod. Phys.* **70,** 685–706 (1998).
2. Cohen-Tannoudji, C. N. Manipulating atoms with photons. *Rev. Mod. Phys.* **70,** 707–719 (1998).
3. Phillips, W. D. Laser cooling and trapping of neutral atoms. *Rev. Mod. Phys.* **70,** 721–741 (1998).
4. Weinstein, J. D., de Carvalho, R., Guillet, T., Friedrich, B. & Doyle, J. M. Magnetic trapping of calcium monohydride molecules at millikelvin temperatures. *Nature* **395,** 148–150 (1998).
5. Takekoshi, T., Patterson, B. M. & Knize, R. J. Observation of optically trapped cold cesium molecules. *Phys. Rev. Lett.* **81,** 5105–5108 (1998).
6. Band, Y. B. & Julienne, P. S. Ultracold-molecule production by laser-cooled atom photoassociation. *Phys. Rev. A* **51,** R4317–R4320 (1995).
7. Fioretti, A. *et al.* Formation of cold Cs_2 molecules through photoassociation. *Phys. Rev. Lett.* **80,** 4402–4405 (1998).
8. Nikolov, A. N. *et al.* Observation of ultracold ground-state potassium molecules. *Phys. Rev. Lett.* **82,** 703–706 (1999).
9. Bethlem, H. L., Berden, G. & Meijer, G. Decelerating neutral dipolar molecules. *Phys. Rev. Lett.* **83,** 1558–1561 (1999).
10. Bethlem, H. L., Berden, G., van Roij, A. J. A., Crompvoets, F. M. H. & Meijer, G. Trapping neutral molecules in traveling potential well. *Phys. Rev. Lett.* **84,** 5744–5747 (2000).
11. Doyle, J. M. & Friedrich, B. Molecules are cool. *Nature* **401,** 749–751 (1999).
12. Williams, C. J. & Julienne, P. S. Molecules at rest. *Science* **287,** 986–987 (2000).
13. Wynar, R., Freeland, R. S., Han, D. J., Ryu, C. & Heinzen, D. J. Molecules in a Bose-Einstein condensate. *Science* **287,** 1016–1019 (2000).
14. Herschbach, D. Molecular clouds, clusters, and corrals. *Rev. Mod. Phys.* **71,** S411–S418 (1999).
15. Maddi, J. A., Dinneen, T. P. & Gould, H. Slowing and cooling molecules and neutral atoms by time-varying electric-field gradients. *Phys. Rev. A* **60,** 3882–3891 (1999).
16. Gupta, M. & Herschbach, D. A mechanical means to produce intense beams of slow molecules. *J. Phys. Chem. A* **103,** 10670–10673 (1999).
17. Friedrich, B. Slowing of supersonically cooled atoms and molecules by time-varying nonresonant induced dipole forces. *Phys. Rev. A* **61,** 025403-1/4 (2000).

18. Friedrich, B. *et al.* Towards magnetic trapping of molecules. *J. Chem. Soc. Faraday Trans.* **94,** 1783–1791 (1998).
19. Wing, W. H. Electrostatic trapping of neutral atomic particles. *Phys. Rev. Lett.* **45,** 631–634 (1980).
20. Gandhi, S. R. & Bernstein, R. B. Focusing and state selection of NH_3 and OCS by the electrostatic hexapole via first- and second-order Stark effects. *J. Chem. Phys.* **87,** 6457–6467 (1987).
21. Ashfold, M. N. R., Dixon, R. N., Little, N., Stickland, R. J. & Western, C. M. The B^1E'' state of ammonia: sub-Doppler spectroscopy at vacuum ultraviolet energies. *J. Chem. Phys.* **89,** 1754–1761 (1988).
22. Bahns, J. T., Gould, P. L. & Stwalley, W. C. Formation of cold ($T \leq 1$ K) molecules. *Adv. At. Mol. Opt. Phys.* **42,** 171–224 (2000).

Acknowledgements

This work is part of the research program of the 'Stichting voor Fundamenteel Onderzoek der Materie (FOM)', which is financially supported by the 'Nederlandse Organisatie voor Wetenschappelijk Onderzoek (NWO)'. The research of R.T.J. has been made possible by a fellowship of the Royal Netherlands Academy of Arts and Sciences. We acknowledge the technical assistance of Ch. Timmer.

Correspondence and requests for information should be addressed to G.M. (e-mail: gerardm@rijnh.nl).

Quasi-planar nucleus structure in apoferritin crystallization

S.-T. Yau* & Peter G. Vekilov*†

* *Center for Microgravity and Materials Research, and* †*Department of Chemistry, University of Alabama in Huntsville, Huntsville, Alabama 35899, USA*

First-order phase transitions of matter, such as condensation and crystallization, proceed through the formation and subsequent growth of 'critical nuclei' of the new phase. The thermodynamics and kinetics of the formation of these critical nuclei depend on their structure, which is often assumed to be a compact, three-dimensional arrangement of the constituent molecules or atoms[5,6]. Recent molecular dynamics simulations have predicted compact nucleus structures for matter made up of building blocks with a spherical interaction field[7,8], whereas strongly anisotropic, dipolar molecules may form nuclei consisting of single chains of molecules[9]. Here we show, using direct atomic force microscopy observations, that the near-critical-size clusters formed during the crystallization of apoferritin, a quasi-spherical protein, and which are representative of the critical nucleus of this system, consist of planar arrays of one or two monomolecular layers that contain 5–10 rods of up to 7 molecules each. We find that these clusters contain between 20 and 50 molecules each, and that the arrangement of the constituent molecules is identical to that found in apoferritin crystals. We anticipate that similarly unexpected critical nucleus structures may be quite common, particularly with anisotropic molecules, suggesting that advanced nucleation theories should treat the critical nucleus structure as a variable.

Protein crystallization is a convenient model for studies of molecular structures and dynamics of nucleation: protein molecules' sizes (a few nanometres) and the typical timescales for growth (a few seconds between sequential discrete growth events) are within the reach of current surface characterization techniques. The molecules of our model, apoferritin[10], are quasi-spherical and consist of 24 subunits arranged in pairs along the 12 walls of a quasi-rhombododecahedron[11,12]. Apoferritin crystals have a face-centred cubic (f.c.c.) lattice, faceted by hexagonal [111] planes[13,14].

We monitored large crystals for periods of several hours in the range of supersaturations σ from 0.5 to 1.6 (for experimental procedures and definition of σ, see Methods below), and detected clusters landing on the top (111) crystal surfaces. Figures 1a and 2a, taken a few minutes after cluster landing, show examples representative of more than 15 such events. In all cases, the molecules in a cluster are arranged in rows of 4–8 molecules, while 3–7 rows assemble in planar domains with an additional 2–3 rows forming a second layer. The cluster in Fig. 1 contains two domains linked by a longer row of about 10 molecules. The centre-to-centre distance between adjacent molecules in a row is 13 nm, equal to that along the close-packed ⟨110⟩ direction in the crystal. Furthermore, one of the molecular rows of the cluster in Fig. 2 generates a new (111) layer that spreads on the crystal surface to meet the crystal's own layer. Hence, these are clusters of apoferritin molecules, which, unlike occurrences in other systems[15,16], have the same arrangement as in the crystal.

The quasi-planar cluster shape precludes the clusters being pieces chopped off a large crystal. We conclude that the clusters form in the solution bulk and then land on the monitored surface because: (1) the clusters consist of (110) planes (Fig. 1f) rather than (111) planes, typical of 'two-dimensional' nuclei of new layers replicating the (111) molecular arrangement of the crystal surface[14]. (2) The molecular rows in the cluster in Fig. 1 are at an angle to the crystal's ⟨110⟩ direction. (3) The cluster and the layer originating from it in Fig. 2 are out of registry with the crystal's own layer causing a boundary free of molecules or consisting of strained molecules. (4) Often—see for instance Fig. 1e—the clusters are pushed back into the solution by the advancing crystal layers. (5) If trapped by the crystal layers[17], as in Fig. 2e and f, a misfit boundary between the two structures appears. Did the cluster structure change after landing, under the influence of the translationally symmetric force exerted by the underlying crystal? It seems not: we would expect that in such a case there would be an exact match and continuity between the structures of the cluster and the underlying crystal, as observed before[15,18].

Figures 1 and 2 show that molecules attach to, and detach from, the cluster between two frames. The attachment and detachment frequencies are comparable, which is unusual for the supersaturated conditions of the observation (we note the fast advancing long straight steps in Fig. 1d and e, and Fig. 2e and f). Comparable rates of molecular attachment and detachment, and bifurcation of their subsequent evolution into either growth or dissolution were observed for all clusters of such sizes seen in our experiments. Estimating the average net frequency of molecular attachment in Fig. 1, we get about 4 molecules/43 s $\approx 0.1\ s^{-1}$ for the approximately 20 possible attachment sites at the ends of the molecular rows, or $0.005\ s^{-1}$ per attachment site. This frequency is more than an order of magnitude lower than the net frequency of attachment to a growth site on the surface of a large crystal—$0.065\ s^{-1}$ (ref. 14). The ratio of the two rates indicates that the size of the cluster in Fig. 1 is just above the critical size. The cluster in Fig. 2 loses one layer of 6 molecules in 896 s (compare Fig. 2a and d). Hence, its size must be just below the critical for that supersaturation. We conclude that these are near-critical-size clusters for the phase transformation occurring in the system, crystallization of apoferritin. Their sizes are, respectively, larger and smaller than the critical, and their structure should be representative of the structure of the nucleus.

The size of the near-critical cluster in Fig. 2 at $\sigma = 1.6$ decreases from about 25 to about 20 molecules during the monitoring time. This cluster is smaller than the one in Fig. 1 at $\sigma = 1.1$ which contains about 50–60 molecules. On the average, smaller near-critical clusters were observed at higher supersaturations. Although we do not have sufficient statistics for a quantitative statement, these observations agree with the predictions of the classical and advanced treatments of nucleation[1,2,19].

To eliminate possible effects of the large crystals on the nucleation pathways, we viewed the glass bottom of the atomic force microscope (AFM) cell before the formation of any crystals at σ between 0.5 and about 2.5. A disordered apoferritin layer with roughly hexagonal molecular co-ordination covers the glass. We saw numer-